



ACADEMIC
PRESS

Available online at www.sciencedirect.com

SCIENCE @ DIRECT®

Journal of Sound and Vibration 261 (2003) 583–612

JOURNAL OF
SOUND AND
VIBRATION

www.elsevier.com/locate/jsvi

An advanced time approach for acoustic analogy predictions

D. Casalino*

*Laboratoire de Mécanique des Fluides et Acoustique, Ecole Centrale de Lyon, Avenue Guy de Collongue,
69131 Ecully Cedex, France*

Received 10 December 2001; accepted 1 May 2002

Abstract

This paper deals with a new interpretation of the retarded time approach that is widely used in the prediction of acoustic fields from moving sources.

A hierarchical inversion between the emission time and the reception time leads to advanced time approach. This consists in projecting the current status of a source in the observer time domain where the received signal is progressively built.

The practical relevance of this methodology lies on two statements: no retarded time equations must be solved; an aerodynamic noise prediction can be processed parallelly to the aerodynamic computation.

Theoretically, the advanced time approach differs from the retarded time approach only in one aspect. A signal emitted at a given instant by a point source, moving at subsonic as well as supersonic velocity, is received only one time by an observer moving at subsonic velocity. Consequently, only one value of the advanced time corresponds to a value of the emission time. The advanced time approach is herein applied to a retarded time solution of the Ffowcs Williams and Hawkings equation proposed by Farassat. The noise radiated by elementary acoustic sources in complex motion is then computed and checked against analytical solutions.

© 2002 Elsevier Science Ltd. All rights reserved.

1. Introduction

Two strategies can be adopted for the prediction of acoustic fields, one based on the Computational AeroAcoustic approach (CAA), the other based on integral formulations. CAA methods consist in solving the flow governing equations including acoustic fluctuations by means of classical CFD methods (finite difference, finite volume, finite elements, etc.) with high-accuracy (low dispersion) numerical schemes. Therefore, reasonable cost solutions are restricted to

*Tel.: +33-472-18-65-39; fax: +33-472-18-91-43.

E-mail address: damiano.casalino@ec-lyon.fr (D. Casalino).

nearfield predictions. On the contrary, integral methods allow one to propagate a nearfield information to the far field at a computational cost that does not depend on the observation distance. The nearfield information can be obtained by means of the integral method itself, as in boundary element methods (BEM), or by means of a CFD/CAA method, as in a hybrid approach.

Hybrid methods are the domain of the acoustic analogy approach. This approach is based on the ideal assumption of separating the sound generation mechanisms from its pure propagation. Therefore, the flow governing equations are arranged in the form of a wave equation where all the terms discarded by the wave propagation pattern are gathered at the right-hand side and interpreted as source terms. Depending on both the reference wave equation and the mechanism that generates the pressure disturbances (free turbulent flows, turbulent flows bounded by solid surfaces, etc.), the acoustic analogy approach leads to different formulations. The first model was proposed by Lighthill [1] and describes the noise generated by a turbulent portion of fluid in an otherwise quiescent unbounded medium. Later on, Lighthill's model was extended by Ffowcs Williams and Hawkings [2] (FW–H) to flows confined by surfaces in arbitrary motion (see Fig. 1).

The FW–H analogy is the most appropriate theoretical support for understanding the mechanisms involved in the generation of aerodynamic sound from bodies in complex motion. This is typically the case of helicopter rotors. The rotating wing of a helicopter generates aerodynamic noise by different mechanisms: the blade thickness, steady and unsteady blade loadings, rotating shocks, blade–vortex interactions, blade–turbulence interactions. In the FW–H equation, these mechanisms appear as source terms of an inhomogeneous wave equation.

The first solutions of the FW–H wave equation were obtained by integrating the pressure field upon the physical surface of the body. This strategy confines all the flow non-linearities into a volume integral extended over a domain exterior to the body. Because of the computational cost required by an accurate prediction of this volume integral, for several years only the linear effects due to the body thickness and aerodynamic loading have been predicted by means of the FW–H analogy. This approximation is valid only at low Mach numbers.

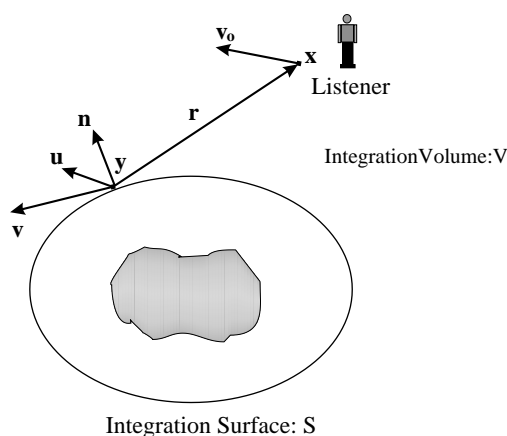


Fig. 1. Scheme of the FW–H acoustic analogy. The flow field enclosed by the integration surface S is replaced by a quiescent fluid ($\rho_0, p_0, \mathbf{u} = 0$). The vectors \mathbf{u} and \mathbf{v} denote the flow velocity and the velocity of the integration surface, respectively. The listener \mathbf{x} moves at the constant velocity \mathbf{v}_0 .

An important source of rotor noise is indeed related to the compressibility effects occurring in the blade tip region. At values of the advancing tip Mach number higher than ~ 0.85 , shock waves appear in the flow field around the rotor, which generate an annoying impulsive noise. A prediction of the so-called High-Speed Impulsive (HSI) noise requires the non-linear effects to be taken into account in the FW–H analogy. An alternative to the computation of the volume term in the FW–H equation consists in using methods based on Kirchhoff's theorem. These methods relate the acoustic field to the pressure field upon a control surface enclosing the blade and *all* the near-blade flow non-linearities. As in the FW–H analogy, a CFD computation provides the flow data upon the integration surface.

For several years, the Kirchhoff formulations have been considered as an ineluctable alternative to the FW–H analogy in the prediction of high-speed rotor noise. More recently, di Francescantonio [3] has shown that the FW–H analogy can be extended to a penetrable control surface and that the surface integrals account for all the non-linear terms enclosed by the integration surface. In response to di Francescantonio [3], Brentner and Farassat [4] pointed out that, although di Francescantonio was the first to apply the FW–H analogy to a Kirchhoff-type integration surface, Ffowcs Williams had already described several implications of a penetrable surface formulation. Moreover, Brentner and Farassat discussed in great detail the conceptual difference between a Kirchhoff formulation and an FW–H penetrable formulation. Their analysis is an example of both elegance and effectiveness. It shows that, since a Kirchhoff equation is related to the linear wave equation, its application to acoustic analogy predictions requires the integration surface to be placed in the linear flow region. On the contrary, since an FW–H equation is an exact rearrangement of the flow governing equations, the placement of the integration surface is only a matter of convenience as long as the quadrupole sources are taken into account by the surface integration. Thus, the FW–H analogy allows accurate noise predictions even when the control surface is not in the linear flow region.

This paper is concerned with a retarded time integral solution of the FW–H equation. The mathematical formalism is that of Farassat and Succi [5] and Brentner [6], extended to a moving observer. A penetrable surface formulation is considered as proposed by di Francescantonio [3] and Brentner and Farassat [4].

The retarded time formulation is hereafter interpreted as an advanced time formulation. This allows the computation of the acoustic field as the CFD simulation is processed. The advanced time approach offers the following advantages:

- (1) Since the acoustic time step is typically several orders of magnitude greater than the aerodynamic time step, the computational time for the noise prediction at each acoustic time step may be smaller than that required by the CFD simulation to cover an acoustic time step. In this case, provided that a parallel architecture is used, the acoustic prediction has a negligible computational cost.
- (2) The advanced time is an algebraic function of the observer and source location at the emission time. Therefore, no iterative solutions of the retarded time equation must be performed at each time step.
- (3) The advanced time projection of the current source status at a given time is univocal. Thus, the application of the advanced time formulation to sources in supersonic motion does not require a modification of the computational algorithms.

- (4) No disk-recording of the flow time history is necessary for the purpose of the acoustic computation.

This new aeroacoustic methodology is implemented in the rotor noise prediction code *Advantia*, developed by the author.

2. FW–H acoustic analogy

Unsteady flows generate pressure fluctuations that partially propagate as acoustic waves within the fluid medium. Lighthill's [1] acoustic analogy separates the sound generation mechanisms from its propagation by arranging the flow governing equations in the form of a wave equation.

The FW–H equation is the most general form of Lighthill's acoustic analogy and can be derived by embedding the exterior flow problem in unbounded space by using generalized functions to describe the flow field.

Let $f(\mathbf{x}, t) = 0$ be a control surface whose points move at the velocity $\mathbf{v}(\mathbf{x}, t)$. The surface $f = 0$ is defined such that $\nabla f = \hat{\mathbf{n}}$, where $\hat{\mathbf{n}}$ denotes the unit normal vector which points out of the surface. Using generalized flow variables, the flow field portion enclosed by the surface, say $f < 0$, can be replaced by a quiescent fluid and a surface distribution of sources which restore the conservative character of the field. Therefore, the continuity and the linear momentum equations can be written as (see Appendix C for the nomenclature)

$$\frac{\partial}{\partial t}[(\rho - \rho_0)\mathbf{H}(f)] + \frac{\partial}{\partial x_i}[\rho u_i \mathbf{H}(f)] = Q\delta(f) \quad (1)$$

with

$$Q = \rho_0 U_i \hat{n}_i \quad \text{and} \quad U_i = \left(1 - \frac{\rho}{\rho_0}\right) v_i + \frac{\rho u_i}{\rho_0}$$

and

$$\frac{\partial}{\partial t}[\rho u_i \mathbf{H}(f)] + \frac{\partial}{\partial x_j}[(\rho u_i u_j + P_{ij})\mathbf{H}(f)] = L_i \delta(f) \quad (2)$$

with

$$L_i = P_{ij} \hat{n}_j + \rho u_i (u_n - v_n) \quad \text{and} \quad P_{ij} = (p - p_0)\delta_{ij} - \tau_{ij},$$

where $Q\delta(f)$ and $L_i\delta(f)$ denote surface source distributions of mass and linear momentum, respectively. Arranging Eqs. (1) and (2) leads to the FW–H equation

$$\square^2\{(\rho - \rho_0)c^2\mathbf{H}(f)\} = \frac{\partial^2}{\partial x_i \partial x_j}\{T_{ij}\mathbf{H}(f)\} - \frac{\partial}{\partial x_i}\{L_i\delta(f)\} + \frac{\partial}{\partial t}\{Q\delta(f)\}, \quad (3)$$

where

$$T_{ij} = \rho u_i u_j + (p' - c^2 \rho')\delta_{ij} - \tau_{ij} \quad (4)$$

is the well-known Lighthill's stress tensor. If the density perturbations are small, as usually happens at the observation distances, the term $(\rho - \rho_0)c^2$ can be replaced by p' and Eq. (3) can be interpreted as an inhomogeneous wave equation for the acoustic pressure p' .

In the aeroacoustic literature, the three source terms on the right-hand side of Eq. (3) are known as the quadrupole, loading and thickness source terms, respectively. The thickness and loading source terms are surface distributions of sources, as indicated by $\delta(f)$. When the control surface encloses a physical surface, the thickness source accounts for the displacement of fluid produced by the body and the loading source accounts for the unsteady loading exerted by the body on the fluid. The quadrupole source, on the other hand, is a volume distribution of sources, as indicates by $H(f)$. The quadrupole source accounts for all the flow non-linearity in the domain exterior to the control surface. When a body moves in an otherwise quiescent fluid, these non-linearities are generated by the body itself and consist of vortical disturbances, shocks and local sound speed variations.

3. Farassat and Brentner retarded time solutions

The FW–H Eq. (3) is an exact rearrangement of the continuity and momentum equation generalized to an unbounded fluid. The flow field enclosed by a control surface is replaced by an elementary flow ($\rho = \rho_0$ and $u_i = 0$) and fulfilment of the flow governing equations is ensured by surface source distributions which ultimately act as sources of sound. Physical surfaces possibly enclosed by the control surface have been removed. Hence, the free-space Green function can be used to convolute Eq. (3). This is defined as $G = \delta(g)/r$, where $g = t - \tau - r/c$ and $r = |\mathbf{x} - \mathbf{y}|$. Here \mathbf{x} and t are the observer position and the observer (reception) time, respectively, whereas \mathbf{y} and τ are the source position and the source (emission) time, respectively. The formal solution of Eq. (3) is thus given by

$$\begin{aligned}
 4\pi p' = & \frac{\partial^2}{\partial x_i \partial x_j} \int \int_{f>0} \frac{\delta(t - \tau - r/c)}{r} T_{ij} dV d\tau \\
 & - \frac{\partial}{\partial x_i} \int \int_{f=0} \frac{\delta(t - \tau - r/c)}{r} L_i dS d\tau \\
 & + \frac{\partial}{\partial t} \int \int_{f=0} \frac{\delta(t - \tau - r/c)}{r} Q dS d\tau,
 \end{aligned} \tag{5}$$

where the properties of the δ -function have been exploited in order to reduce volume integrals to corresponding surface integrals. A change of the integration variable within the integral expressions is carried out by using the well-known formula

$$\int \mathcal{Q}(\tau) \delta(g(\tau)) = \sum_{n=1}^N \frac{\mathcal{Q}}{|\partial g / \partial \tau|}(\tau_{ret}^n) \tag{6}$$

the sum being taken over all the zeros τ_{ret}^n of the *retarded time equation* $g = 0$. When the source is in subsonic motion, there exists one and only one solution of the retarded time equation at any reception time. Conversely, when the source is in supersonic motion, more than one solution may exist. This physically accounts for the fact that signals emitted at different times can be detected at the same time. The time-source derivative of g is

$$\frac{\partial g}{\partial \tau} = -1 + M_r, \tag{7}$$

where $M_r = M_i \hat{r}_i$ is the component of the source Mach number vector in the direction of the observer, $\hat{r}_i = (x_i - y_i)/r$ denoting the unit vector in the radiation direction. The term $|1 - M_r|$ accounts for a dilatation or contraction of the observer time scale with respect to the source time scale, depending on whether the source moves far away from or towards the observer, respectively. This effect is known as *Doppler effect*.

Suppose that the source elements in Eq. (5) are in subsonic motion and denote as $[\dots]_{ret}$ the evaluation at the retarded time

$$\tau_{ret} = t - \frac{|\mathbf{x} - \mathbf{y}(\tau_{ret})|}{c}. \quad (8)$$

Then, applying Eqs. (6) and (7) to the integral expression (5) yields

$$\begin{aligned} 4\pi p' = & \frac{\partial^2}{\partial x_i \partial x_j} \int_{f>0} \left[\frac{T_{ij}}{r(1 - M_r)} \right]_{ret} dV \\ & - \frac{\partial}{\partial x_i} \int_{f=0} \left[\frac{L_i}{r(1 - M_r)} \right]_{ret} dS \\ & + \frac{\partial}{\partial t} \int_{f=0} \left[\frac{Q}{r(1 - M_r)} \right]_{ret} dS. \end{aligned} \quad (9)$$

This is the retarded time solution of the FW–H equation (3). It is interesting to notice that the change of variable used to integrate the Dirac delta function $\delta(g)$ provides a singular behaviour at the transonic condition $M_r = 1$. Fortunately, this singularity can be removed by applying a different change of variable. The reader is reminded to the comprehensive work of Farassat [7] for a description of these different formulations. Furthermore, the work of Ardavan [8] can be read for a discussion on the nature of the transonic singularity.

Starting from Eq. (9), different expressions of the retarded time formulation can be obtained in order to improve the practical relevance of the FW–H analogy. A first modification consists in transforming the space derivatives into time derivatives. This is done by using the relation

$$\frac{\partial}{\partial x_i} \int_{f=0} \left[\frac{L_i}{r(1 - M_r)} \right]_{ret} dS = -\frac{1}{c} \frac{\partial}{\partial t} \int_{f=0} \left[\frac{L_i \hat{r}_i}{r(1 - M_r)} \right]_{ret} dS - \int_{f=0} \left[\frac{L_i \hat{r}_i}{r^2(1 - M_r)} \right]_{ret} dS \quad (10)$$

for the loading noise, and twice the same chain for the quadrupole noise. Hence, it follows that

$$\begin{aligned} 4\pi p' = & \frac{1}{c^2} \frac{\partial^2}{\partial t^2} \int_{f>0} \left[\frac{T_{rr}}{r(1 - M_r)} \right]_{ret} dV + \frac{1}{c} \frac{\partial}{\partial t} \int_{f>0} \left[\frac{3T_{rr} - T_{ii}}{r^2(1 - M_r)} \right]_{ret} dV + \int_{f>0} \left[\frac{3T_{rr} - T_{ii}}{r^3(1 - M_r)} \right]_{ret} dV \\ & + \frac{1}{c} \frac{\partial}{\partial t} \int_{f=0} \left[\frac{L_i \hat{r}_i}{r(1 - M_r)} \right]_{ret} dS + \int_{f=0} \left[\frac{L_i \hat{r}_i}{r^2(1 - M_r)} \right]_{ret} dS \\ & + \frac{\partial}{\partial t} \int_{f=0} \left[\frac{Q}{r(1 - M_r)} \right]_{ret} dS. \end{aligned} \quad (11)$$

A second modification consists in moving the time derivative inside the integrals. As demonstrated by Farassat and Succi [5] and Brentner [6], this can be made by using the rule

$$\frac{\partial}{\partial t} \Big|_{\mathbf{x}} = \left[\frac{1}{1 - M_r} \frac{\partial}{\partial \tau} \Big|_{\mathbf{x}} \right]_{ret} \quad (12)$$

together with the relations

$$\frac{\partial r}{\partial \tau} = -cM_r, \tag{13}$$

$$\frac{\partial \hat{r}_i}{\partial \tau} = \frac{\hat{r}_i c M_r - c M_i}{r}, \tag{14}$$

$$\frac{\partial M_r}{\partial \tau} = \frac{1}{r} \left\{ \hat{r}_i \frac{\partial M_i}{\partial \tau} + c(M_r^2 - M^2) \right\}. \tag{15}$$

It finally results that

$$p'(\mathbf{x}, t) = p'_Q(\mathbf{x}, t) + p'_L(\mathbf{x}, t) + p'_T(\mathbf{x}, t), \tag{16}$$

where the expressions of the thickness (Q), loading (L) and quadrupole (T) noise are reported below.

Thickness noise

$$4\pi p'_Q(\mathbf{x}, t) = \int_{f=0} \left[\frac{\rho_0(\dot{U}_n + U_{\dot{n}})}{r(1 - M_r)^2} \right]_{ret} dS + \int_{f=0} \left[\frac{\rho_0 U_n (r\dot{M}_r + c(M_r - M^2))}{r^2(1 - M_r)^3} \right]_{ret} dS \tag{17}$$

where \mathbf{M} is the Mach number vector of a source point on the integration surface, and the remaining terms are defined as

$$\begin{aligned} U_n &= U_i \hat{n}_i, & U_{\dot{n}} &= U_i \dot{\hat{n}}_i, & \dot{U}_n &= \dot{U}_i \hat{n}_i, \\ M_r &= M_i \hat{r}_i, & \dot{M}_r &= \dot{M}_i \hat{r}_i. \end{aligned} \tag{18}$$

Dots on quantities denote time derivative with respect to the source time τ . All the involved quantities are described in Appendix B.

Loading noise

$$4\pi p'_L(\mathbf{x}, t) = \frac{1}{c} \int_{f=0} \left[\frac{\dot{L}_r}{r(1 - M_r)^2} \right]_{ret} dS + \int_{f=0} \left[\frac{L_r - L_M}{r^2(1 - M_r)^2} \right]_{ret} dS + \frac{1}{c} \int_{f=0} \left[\frac{L_r (r\dot{M}_r + c(M_r - M^2))}{r^2(1 - M_r)^3} \right]_{ret} dS, \tag{19}$$

where

$$L_r = L_i \hat{r}_i, \quad \dot{L}_r = \dot{L}_i \hat{r}_i, \quad L_M = L_i M_i. \tag{20}$$

Quadrupole noise

$$4\pi p'_T(\mathbf{x}, t) = \int_{f>0} \left[\frac{K_1}{c^2 r} + \frac{K_2}{c r^2} + \frac{K_3}{r^3} \right]_{ret} dV \tag{21}$$

with

$$\begin{aligned}
 K_1 &= \frac{\ddot{T}_{rr}}{(1-M_r)^3} + \frac{\ddot{M}_r T_{rr} + 3\dot{M}_r \dot{T}_{rr}}{(1-M_r)^4} + \frac{3\dot{M}_r^2 T_{rr}}{(1-M_r)^5}, \\
 K_2 &= \frac{-\dot{T}_{ii}}{(1-M_r)^2} - \frac{4\dot{T}_{Mr} + 2T_{\dot{M}_r} + \dot{M}_r T_{\dot{i}i}}{(1-M_r)^3} \\
 &\quad + \frac{3\{(1-M^2)\dot{T}_{rr} - 2\dot{M}_r T_{Mr} - M_i \dot{M}_i T_{rr}\}}{(1-M_r)^4} + \frac{6\dot{M}_r(1-M^2)T_{rr}}{(1-M_r)^5}, \\
 K_3 &= \frac{2T_{MM} - (1-M^2)T_{ii}}{(1-M_r)^3} - \frac{6(1-M^2)T_{Mr}}{(1-M_r)^4} + \frac{3(1-M^2)^2 T_{rr}}{(1-M_r)^5}, \tag{22}
 \end{aligned}$$

where $T_{rr} = T_{ij}\hat{r}_i\hat{r}_j$ is the double contraction of the Lighthill stress tensor T_{ij} , and the other terms are defined as

$$\begin{aligned}
 T_{MM} &= T_{ij}M_iM_j, & T_{Mr} &= T_{ij}M_i\hat{r}_j, & T_{\dot{M}_r} &= T_{ij}\dot{M}_i\hat{r}_j, \\
 \dot{T}_{Mr} &= \dot{T}_{ij}M_i\hat{r}_j, & \dot{T}_{rr} &= \dot{T}_{ij}\hat{r}_i\hat{r}_j, & \ddot{T}_{rr} &= \ddot{T}_{ij}\hat{r}_i\hat{r}_j.
 \end{aligned} \tag{23}$$

In Eq. (22), \mathbf{M} is the Mach number vector of a volume source fixed in the body reference frame.

The above expression of the quadrupole noise is equivalent to that obtained by Brentner [6], with the difference that in Brentner's paper the volume integral in Eq. (21) is carried out in two stages. First, an integration of the aerodynamic quantity T_{ij} in the direction normal to the rotor disk is performed, providing the quantity

$$Q_{ij} = \int_{f>0} T_{ij} dz, \tag{24}$$

which does not depend on the observer position. Second, an integration on the rotor disk is performed by using the same expressions as in Eq. (22), but with Q_{ij} at the place of T_{ij} . This approximation is justified by the fact that the helicopter transonic HSI-noise is maximum for an observation point in the plane of the rotor. In this case, provided that the observer is in the far field, Brentner's procedure is rigorous.

A final modification consists in extending the integral formulation to an observer moving at the constant velocity $c\mathbf{M}_o$. This can be done by interpreting the time derivative related to the thickness noise in Eq. (11) as a Lagrangian derivative. The other time derivatives, in fact, have been obtained by using the relation (12) where derivatives are taken at fixed observer position. Thus, it results that

$$4\pi p'_Q(\mathbf{x}, t) = \frac{\partial}{\partial t} \int_{f=0} \left[\frac{\rho_0 U_n}{r(1-M_r)} \right]_{ret} dS + cM_{oi} \frac{\partial}{\partial x_i} \int_{f=0} \left[\frac{\rho_0 U_n}{r(1-M_r)} \right]_{ret} dS.$$

Proceeding as in Eq. (10) to translate the space derivatives into a time derivative yields

$$\begin{aligned}
 4\pi p'_Q(\mathbf{x}, t) &= \frac{\partial}{\partial t} \int_{f=0} \left[\frac{\rho_0 U_n}{r(1-M_r)} \right]_{ret} dS \\
 &\quad - \frac{\partial}{\partial t} \int_{f=0} \left[\frac{\rho_0 U_n M_{or}}{r(1-M_r)} \right]_{ret} dS - c \int_{f=0} \left[\frac{\rho_0 U_n M_{or}}{r^2(1-M_r)} \right]_{ret} dS, \tag{25}
 \end{aligned}$$

where $M_{or} = M_{oi}\hat{r}_i$ is the observer Mach number vector in the radiation direction. Finally, moving the time derivative inside the integral yields

Thickness noise for a moving observer

$$\begin{aligned}
4\pi p'_Q(\mathbf{x}, t) = & \int_{f=0} \left[\frac{\rho_0(\dot{U}_n + U_{\dot{n}})}{r(1 - M_r)^2} \right]_{ret} dS \\
& + \int_{f=0} \left[\frac{\rho_0 U_n(r\dot{M}_r + c(M_r - M^2))}{r^2(1 - M_r)^3} \right]_{ret} dS \\
& - \int_{f=0} \left[M_{or} \frac{\rho_0(\dot{U}_n + U_{\dot{n}})}{r(1 - M_r)^2} \right]_{ret} dS - \int_{f=0} \left[M_{or} \frac{\rho_0 \dot{M}_r U_n}{r(1 - M_r)^3} \right]_{ret} dS \\
& - \int_{f=0} \left[\frac{\rho_0 c \{ 2M_{or}M_r - M_{or}M^2 - M_{oi}M_i(1 - M_r) - M_{or}M_r^2 \} U_n}{r^2(1 - M_r)^3} \right]_{ret} dS \\
& - \int_{f=0} \left[\frac{M_{or}\rho_0 c U_n}{r^2(1 - M_r)} \right]_{ret} dS. \tag{26}
\end{aligned}$$

3.1. Non-dimensionalized FW–H integral equation

The formulation coded in *Advantia* is a non-dimensionalized form of Eqs. (26), (19) and (21). In view of interfacing to a finite volume CFD code, the flow field is expressed in conservative variables $(\rho, \rho u_i, \rho E)$, where E is the specific total internal energy. Furthermore, since CFD solutions are commonly computed in a body reference frame, the flow velocity \mathbf{u} is deprived of the velocity \mathbf{v} of the control surface.

Hence, introducing a reference length l_{ref} , velocity U_{ref} , time l_{ref}/U_{ref} and dynamic pressure $p_d = \rho_0 U_{ref}^2/2$, the following non-dimensionalized expressions can be obtained (see Appendix C for notation):

$$\begin{aligned}
\frac{2\pi}{p_d} p'_Q(\mathbf{X}, \tau) = & \int_{f=0} \left[\frac{\dot{V}_i \hat{n}_i + \dot{q}_i \hat{n}_i + (V_i + q_i) \dot{\hat{n}}_i}{R(1 - M_r)^2} + \frac{(V_n + q_n) \{ R\dot{M}_r + ((M_r - M^2)/M_{ref}) \}}{R^2(1 - M_r)^3} \right]_{ret} dS \\
& - \int_{f=0} \left[M_{or} \frac{\dot{V}_i \hat{n}_i + \dot{q}_i \hat{n}_i + (V_i + q_i) \dot{\hat{n}}_i}{R(1 - M_r)^2} \right]_{ret} dS - \int_{f=0} \left[\frac{M_{or} \dot{M}_r (V_i + q_i) \hat{n}_i}{R(1 - M_r)^3} \right]_{ret} dS \\
& - \int_{f=0} \left[\frac{\{ 2M_{or}M_r - M_{or}M^2 - M_{oi}M_i(1 - M_r) - M_{or}M_r^2 \} (V_i + q_i) \hat{n}_i}{M_{ref} R^2(1 - M_r)^3} \right]_{ret} dS \\
& - \int_{f=0} \left[\frac{(V_i + q_i) \hat{n}_i M_{or}}{M_{ref} R^2(1 - M_r)} \right]_{ret} dS, \tag{27}
\end{aligned}$$

$$\begin{aligned}
\frac{2\pi}{p_d} p'_L(\mathbf{X}, \tau) = & \int_{f=0} \left[\frac{M_{ref} \lambda_r}{R(1 - M_r)^2} \right]_{ret} dS + \int_{f=0} \left[\frac{\lambda_r - \lambda_M}{R^2(1 - M_r)^2} \right]_{ret} dS \\
& + \int_{f=0} \left[\frac{M_{ref} \lambda_r \{ R\dot{M}_r + ((M_r - M^2)/M_{ref}) \}}{R^2(1 - M_r)^3} \right]_{ret} dS, \tag{28}
\end{aligned}$$

$$\frac{2\pi}{p_d} p'_T(\mathbf{X}, \tau) = \int_{f>0} \left[M_{ref}^2 \frac{K_1}{R} + M_{ref} \frac{K_2}{R^2} + \frac{K_3}{R^3} \right]_{ret} dV \quad \text{with} \quad (29)$$

$$K_1 = \frac{\ddot{\Psi}_{rr}}{(1 - M_r)^3} + \frac{\ddot{M}_r \Psi_{rr} + 3\dot{M}_r \dot{\Psi}_{rr}}{(1 - M_r)^4} + \frac{3\dot{M}_r^2 \Psi_{rr}}{(1 - M_r)^5},$$

$$K_2 = \frac{-\dot{\Psi}_{ii}}{(1 - M_r)^2} - \frac{4\dot{\Psi}_{Mr} + 2\Psi_{\dot{M}_r} + \dot{M}_r \Psi_{ii}}{(1 - M_r)^3} + \frac{3\{(1 - M^2)\dot{\Psi}_{rr} - 2\dot{M}_r \Psi_{Mr} - M_i \dot{M}_i \Psi_{rr}\}}{(1 - M_r)^4} + \frac{6\dot{M}_r(1 - M^2)\Psi_{rr}}{(1 - M_r)^5}$$

$$K_3 = \frac{2\Psi_{MM} - (1 - M^2)\Psi_{ii}}{(1 - M_r)^3} - \frac{6(1 - M^2)\Psi_{Mr}}{(1 - M_r)^4} + \frac{3(1 - M^2)^2\Psi_{rr}}{(1 - M_r)^5}, \quad (30)$$

where square brackets enclose quantities evaluated at the retarded time θ_{ret} obtained from the dimensionless retarded time equation

$$\theta_{ret} = \theta - (\mathbf{X}(\theta) - \mathbf{Y}(\theta_{ret}))M_{ref}. \quad (31)$$

In this expression, the current time θ is the observer time, whereas θ_{ret} is the retarded source time.

4. The advanced time approach

The retarded time approach consists in evaluating the signal received at a given time t (in a retarded time approach, the computational time is the reception time) through a summation of all the disturbances reaching the observer at the same time t . Depending on the location and velocity of both the source and observer, these disturbances are emitted at different retarded times and cover different distances before to reach the observation point.

In this work, an advanced time approach is proposed. This consists in using a retarded time approach, but from the point of view of the source. Therefore, at a given time the contributions from the integration domain (in an advanced time approach, the computational time is the emission time) are calculated, based on the current aerodynamic data and the current kinematics of the integration domain. At each computational time and for each source element, the time at which the corresponding disturbance will reach the observer is calculated and referred to as *advanced time*. The observer location at the advanced time is used to calculate the relative position between the observer and a point source. The signal is finally built up in the observer time domain through a summation over all the computed contributions.

Let us consider the retarded time equation

$$\tau_{ret} = t - \frac{|\mathbf{x}(t) - \mathbf{y}(\tau_{ret})|}{c}. \quad (32)$$

At an observer time $t + \mathcal{T}$, this yields

$$\tau'_{ret} = t + \mathcal{T} - \frac{|\mathbf{x}(t + \mathcal{T}) - \mathbf{y}(\tau'_{ret})|}{c}. \quad (33)$$

Thus, setting $\tau'_{ret} \equiv t$ leads to

$$\mathcal{T} = \frac{|\mathbf{x}(t + \mathcal{T}) - \mathbf{y}(t)|}{c} \tag{34}$$

The quantity $t + \mathcal{T}$ is the time at which a disturbance emitted by a source element \mathbf{y} at the time t will reach the observer \mathbf{x} . Thus, it is interpreted as the advanced time,

$$t_{adv} = t + \mathcal{T} \tag{35}$$

Suppose that the observer moves at the constant velocity $c\mathbf{M}_o$. Eq. (34) can be solved in \mathcal{T} , providing

$$\begin{aligned} \mathcal{T}^\pm &= \frac{r_i M_{oi} \pm \sqrt{(r_i M_{oi})^2 + r^2(1 - M_o^2)}}{c(1 - M_o^2)} \\ &= \frac{r}{c} \left\{ \frac{M_{or} \pm \sqrt{M_{or}^2 + 1 - M_o^2}}{1 - M_o^2} \right\}, \end{aligned} \tag{36}$$

where $r_i = x_i(t) - y_i(t)$ is the radiation vector and $M_{or} = \hat{r}_i M_{oi}$ is the observer Mach number vector in the radiation direction. Since a signal cannot be received before it is emitted, the quantity \mathcal{T} must be positive. Interestingly, \mathcal{T} depends only on the observer velocity and not on the source velocity. The following cases can be distinguished:

- (a) observer at rest: $M_o = 0$. Only the solution $\mathcal{T}^+ = r/c$ is a physical solution.
- (b) Observer in subsonic motion: $M_o < 1$,

$$M_{or} \pm \sqrt{M_{or}^2 + \alpha^2} > 0, \tag{37}$$

with $\alpha^2 = 1 - M_o^2$. Hence, only the solution \mathcal{T}^+ is a physical solution.

- (c) Observer in supersonic motion: $M_o > 1$

$$M_{or} \pm \sqrt{M_{or}^2 - \alpha^2} < 0, \tag{38}$$

with $\alpha^2 = -1 + M_o^2$. Hence,

- (1) observer moving far away from the source: $M_{or} > 0$. Both solutions \mathcal{T}^\pm do not match the causality condition $\mathcal{T} > 0$;
- (2) observer moving towards the source: $M_{or} < 0$. Both solutions \mathcal{T}^\pm are physical solutions, provided that $M_{or} < -\sqrt{M_o^2 - 1}$.

In the present study, a subsonic observer velocity is supposed. Thus, only the solution \mathcal{T}^+ is considered and the advanced time is given by

$$t_{adv} = t + \frac{r(t)}{c} \left\{ \frac{M_{or}(t) + \sqrt{M_{or}^2(t) + 1 - M_o^2}}{1 - M_o^2} \right\} \tag{39}$$

It is interesting to notice that a source time t corresponds only to one value of the advanced time t_{adv} . This happens for any source velocity. Furthermore, the advanced time expression is given in an explicit form.

The implementation of the advanced time formulation does not require a modification of the source terms in the integrals (27)–(29). However, difficulties may arise in the reconstruction of the signal. Indeed, due to the Doppler effect, an equally spaced discretization of the source time domain does not correspond to an equally spaced discretization of the observer time domain. This can be understood by taking the time derivative of expression (39), i.e.,

$$\frac{dt_{adv}}{dt} = 1 - \frac{M_i - M_{oi}}{1 - M_o^2} \left\{ M_{oi} + \frac{M_{or}M_{oi} + (1 - M_o^2)\hat{r}_i}{\sqrt{M_{or}^2 + 1 - M_o^2}} \right\}, \quad (40)$$

where M_i denotes the source Mach number. Considering, for simplicity, an observer at rest yields

$$\frac{dt_{adv}}{dt} = 1 - M_r \quad (41)$$

and in discretized form

$$t_{adv}^{j+1} = t_{adv}^j + (1 - M_r^j)\Delta t, \quad (42)$$

where Δt is the computational time-step. In Fig. 2, the advanced time is plotted for a fixed observer and a source moving at different velocities v_o along a rectilinear trajectory. The source intercepts the observation point at $t_o = r_o/v_o$, r_o being the initial distance of the source. For $t < t_o$ and subsonic source velocities, the curves have positive slopes, with values $0 < 1 - M_r \leq 1$. This situation corresponds to a contraction of the advanced time scale. For $t < t_o$ and supersonic source velocities, the curves have negative slopes. Thus, signals emitted before are detected after. Finally, for $t > t_o$ the curves have positive slopes, with values $1 - M_r > 1$. This situation corresponds to a dilatation of the advanced time scale. When the computed disturbances are sampled on an equally spaced advanced time domain¹, the following situations can take place:

- (1) only one contribution p_i^j from the source element S_i falls in the interval $[t^j, t^{j+1}]_{adv}$;
- (2) no contribution from the source element S_i is projected in the interval $[t^j, t^{j+1}]_{adv}$;
- (3) more than one contribution $(p_i^j)_n$ from the source element S_i falls in the interval $[t^j, t^{j+1}]_{adv}$.

Since the Doppler factor is already accounted for in the source terms, contributions $(p_i^j)_n$ must not be added, but used to determine a suitable contribution p_i^j . A summation over all the source elements must be made as a final step, namely $p^j = \sum_i p_i^j$, providing the pressure value at the advanced time $j\Delta t$. The procedure used in this work to build on the pressure signal in the advanced time domain is described in Appendix A. It is essentially based on a linear interpolation. Although more accurate schemes can be implemented, the one proposed in this paper is a good compromise between accuracy and simplicity.

5. Assessment of the advanced time approach

In this section the feasibility of an advanced time prediction of the noise from sources in complex subsonic motion is tested. The penetrable FW–H formulation is also validated by

¹The same discretization used in the source computation is used in the advanced time domain.

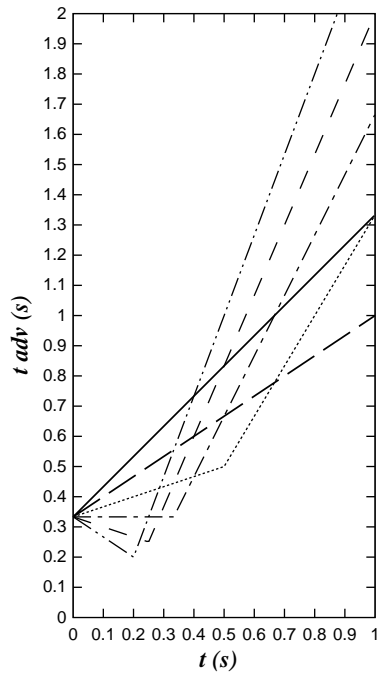


Fig. 2. Advanced time versus current time for a source in constant motion at different Mach numbers in the direction of a fixed observer. The source initial distance from the observer is $r_o = 100$ m and the sound speed is $c_o = 300$ m/s. Source Mach numbers: —, $M_o = 0$; — —, $M_o = 0.33$; - - - -, $M_o = 0.66$, - · - ·, $M_o = 1$; · · · ·, $M_o = 1.33$; · · · · ·, $M_o = 1.67$.

considering monopole sources enclosed by a control surface. Only the linear contributions (27) and (28) are considered.

The following test cases are examined:

- (1) acoustic monopoles translating and rotating with respect to an observer which translates at a constant velocity, as sketched in Fig. 3;
- (2) radial dipoles rotating and translating with respect to a fixed observer, as sketched in Fig. 13 to follow;
- (3) axial dipoles rotating and translating with respect to a fixed observer, as sketched in Fig. 20 to follow.

The first test case is performed in order to validate the penetrable surface formulation and the thickness noise extension to a moving observer. The second and the third test cases are performed in order to show the feasibility of an advanced time prediction of the noise from a high-speed rotor.

The assessment strategy is the following: first, the far field radiated by a set of elementary acoustic sources is obtained directly from analytical expressions and is referred to as *analytical solution*. Second, the analytical solution on a control surface is propagated into the far field by the analogy formulation and is referred to as *numerical solution*. Third, the numerical solution is

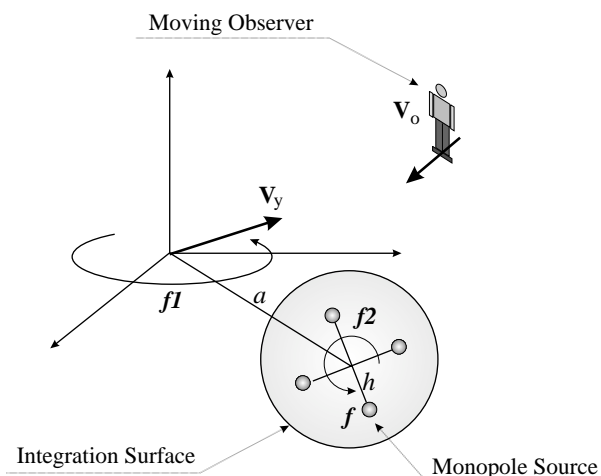


Fig. 3. Scheme of Test 1. A set of equal monopoles are located on the vertices of a regular polygon. They rotate around the axis of the polygon at the frequency f_2 , and around a vertical axis at the frequency f_1 . These two axes of rotation are normal to each other. The system translates at the velocity v_y and the observer translates at the velocity v_o . Surface integration is performed upon a sphere. It encloses the monopoles and rotates around the vertical axis at the frequency f_1 .

compared to the analytical solution. Acoustic monopoles and dipoles in subsonic motion are considered as elementary sources.

5.1. Test 1

Harmonic monopoles of equal amplitude $q = 0.1$ kg/s, phase and frequency f are located on the vertices of a regular polygon. They rotate around the axis of the polygon at the frequency f_2 , and around a vertical axis at the frequency f_1 . The source distances from these normal axes are h and a , respectively. The system translates at the velocity v_y and the observer translates at the velocity v_o . The monopoles are enclosed by a control spherical surface rotating around the vertical axis at the frequency f_1 .

The sound radiated by a moving harmonic monopole and received by a moving observer is used as analytical solution, namely

$$p'(\mathbf{x}, t) = \rho_0 \frac{D}{Dt} \left[\frac{Q(t)}{4\pi r(1 - M_r)} \right]_{ret}, \quad (43)$$

$$u'_i(\mathbf{x}, t) = \frac{\partial}{\partial x_i} \left[\frac{Q(t)}{4\pi r(1 - M_r)} \right]_{ret}, \quad (44)$$

where D/Dt denotes a convective time derivative (see Ref. [9, pp. 269–275]). These expressions provide both the farfield acoustic solution and the *aerodynamic* field on the integration surface². The latter is defined in terms of the acoustic pressure p' , its time derivative \dot{p} , the acoustic velocity

²The term aerodynamic is indeed extended to denote an acoustic field.

u'_i and its time derivative \dot{u}'_i . These quantities are evaluated numerically through a retarded time approach.

Several cases are considered in order to check the following aspects of the formulation:

- (a) the advanced time approach;
- (b) the penetrable control surface formulation;
- (c) the moving observer extension of the thickness noise.

In the present work, no attempt has been made to characterize the numerical accuracy of the spatial discretization. The surface integration is performed upon a sphere of radius 0.5 m, with a polar discretization of 24×24 elements. A Gaussian integration is performed by using 4 points on both quadrangular and triangular elements. A linear isoparametric interpolation is used to define the aerodynamic quantities at the collocation points.

Concerning the time discretization, 200 time steps per acoustic period are initially used for different configurations. Later on, computations are performed for one configuration down to 20 time steps per acoustic period.

The observer initial position is the same for all the presented cases, say $\mathbf{x} = (10, 10, 10)$ m, as well as the rotation radiuses $a = 1$ m and $h = 0.1$ m. The remaining parameters are listed in Table 1.

In Figs. 4–10, numerical results obtained with 200 time steps per acoustic period are checked against the analytical solutions. The plots show that the agreement between the numerical and the analytical solutions is good for all the investigated configurations. The relative

Table 1
Test 1: geometrical and kinematic parameters

	N	f	f_1	f_2	\mathbf{v}_y	\mathbf{v}_o	M_y	M_o	Err_L	Fig.
A	1	100	0	0	(0,0,0)	(0,0,0)	0	0	1.36E−2	4(a)
B	4	110	0	0	(0,0,0)	(0,0,0)	0	0	1.31E−2	4(b)
C	1	100	20	0	(0,0,0)	(0,0,0)	0	0	1.52E−2	5(a)
D	4	110	20	0	(0,0,0)	(0,0,0)	0	0	8.45E−3	5(b)
E	1	100	20	49	(0,0,0)	(0,0,0)	0	0	1.57E−3	6(a)
F	4	110	20	43	(0,0,0)	(0,0,0)	0	0	8.26E−3	6(b)
G	1	100	20	49	(50,40,30)	(0,0,0)	0.76	0	1.88E−2	7(a)
H	4	110	20	43	(50,40,30)	(0,0,0)	0.76	0	6.79E−3	7(b)
I	1	100	20	49	(50,40,30)	(−10,−30,−50)	0.76	0.17	3.34E−5	8(a)
J	4	110	20	43	(50,40,30)	(−10,−30,−50)	0.76	0.17	4.19E−3	8(b)
K	1	100	20	49	(50,40,30)	(−20,−60,−100)	0.76	0.35	2.60E−2	9(a)
L	4	110	20	43	(50,40,30)	(−20,−60,−100)	0.76	0.35	5.79E−4	9(b)
M	1	100	20	49	(100,80,60)	(−10,−30,−50)	0.97	0.17	5.40E−2	10(a)
N	4	110	20	43	(100,80,60)	(−10,−30,−50)	0.97	0.17	9.45E−2	10(b)

N is the number of acoustic monopoles; f is the acoustic frequency; f_1 and f_2 are the rotation frequency around the vertical and the horizontal axes, respectively; \mathbf{v}_y is the forward velocity of the sources; \mathbf{v}_o is the observer translation velocity; M_y is the maximum Mach number of the integration surface; M_o is the observer Mach number; Err_L denotes the relative L-error; Fig. indicates the label of the corresponding figure. All the quantities are expressed in SI units. Computations are performed with a time discretization of 200 time steps per acoustic period.

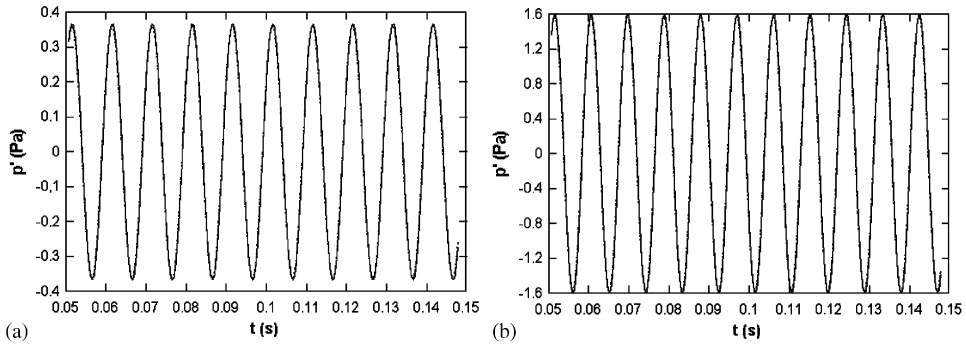


Fig. 4. Test 1. Case A (left) and Case B (right): —, analytical solution; ----, numerical solution.

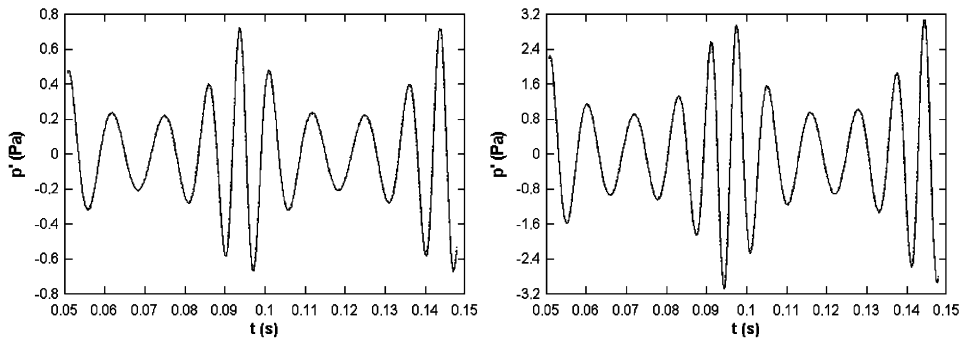


Fig. 5. Test 1. Case C (left) and Case D (right): —, analytical solution; ----, numerical solution.

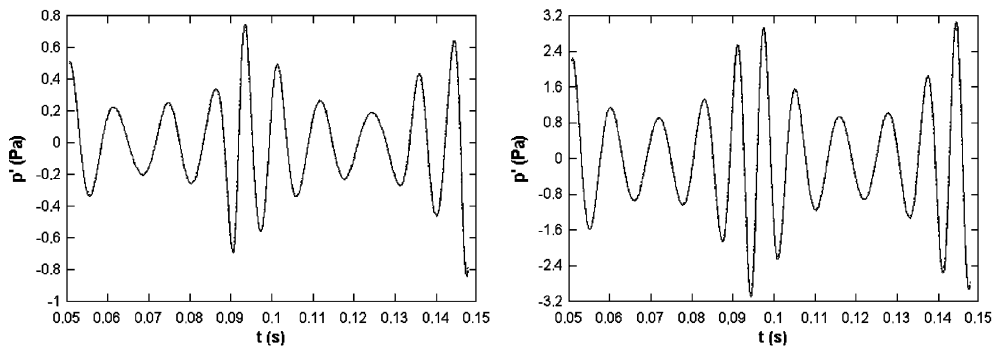


Fig. 6. Test 1. Case E (left) and Case F (right): —, analytical solution; ----, numerical solution.

L-errors, say

$$Err_L = \frac{\max_j |p_{num}^j - p_{an}^j|}{\max_j |p_{an}^j|} \tag{45}$$

for the different configurations are listed in [Table 1](#).

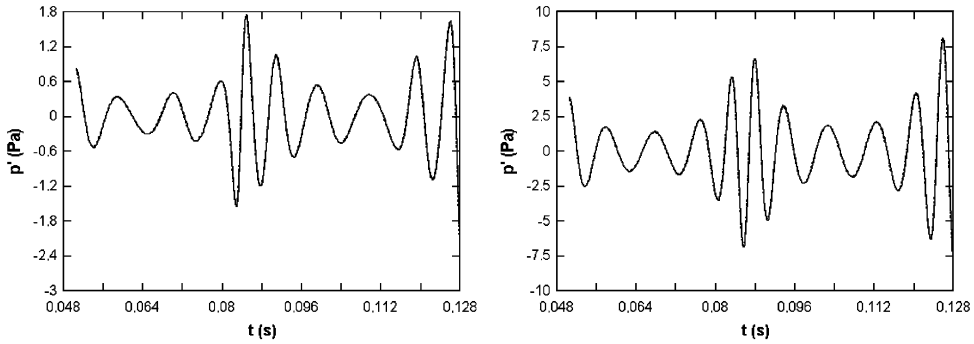


Fig. 7. Test 1. Case G (left) and Case H (right): —, analytical solution; ----, numerical solution.

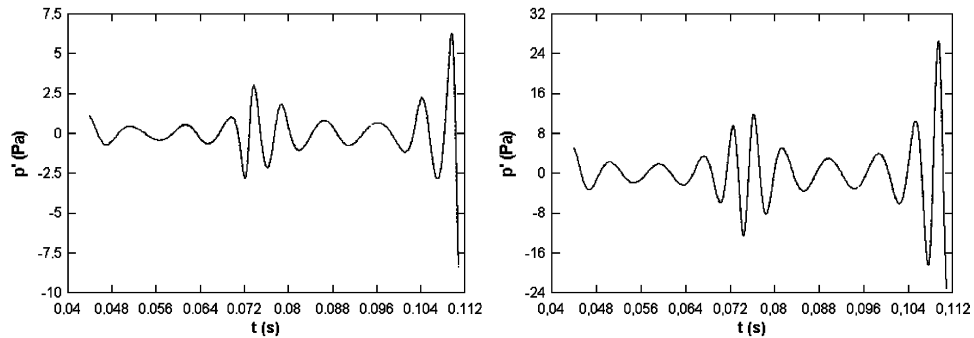


Fig. 8. Test 1. Case I (left) and Case J (right): —, analytical solution; ----, numerical solution.

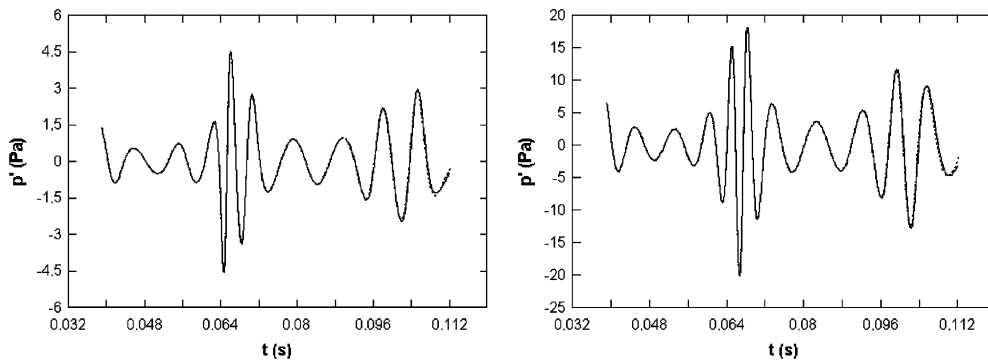


Fig. 9. Test 1. Case K (left) and Case L (right): —, analytical solution; ----, numerical solution.

In Fig. 11, the relative L_2 -error for Case I, say

$$Err_{L2} = \frac{\sum_j (p_{num}^j - p_{an}^j)^2}{\sum_j (p_{an}^j)^2}, \tag{46}$$

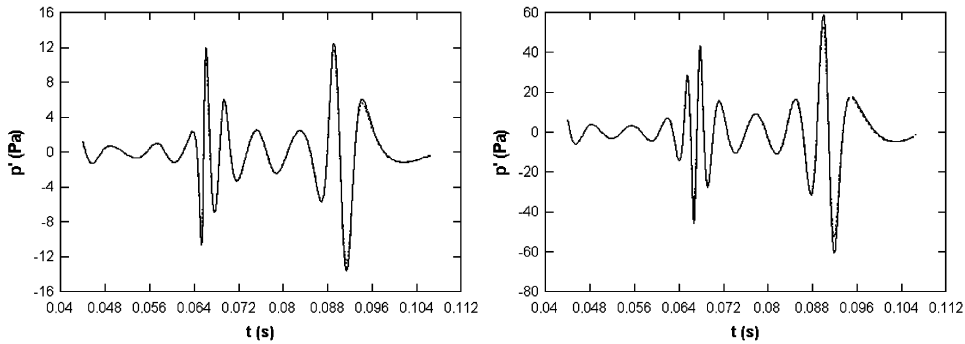


Fig. 10. Test 1. Case M (left) and Case N (right).

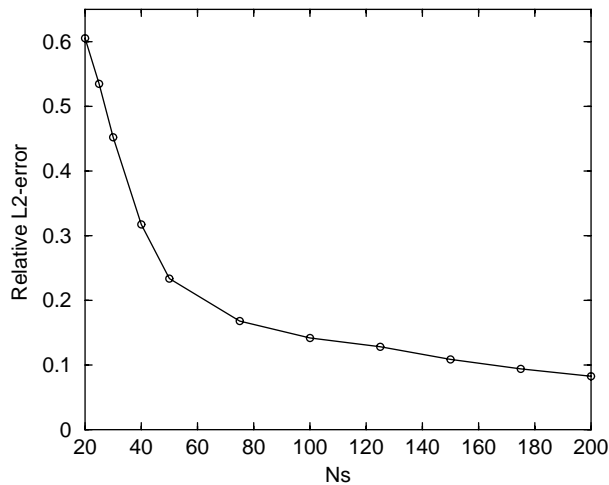


Fig. 11. Test 1, Case I. Relative L_2 -error versus the number of time steps per acoustic period.

is plotted against the number of samples N_s per acoustic period, from $N_s = 20$ up to $N_s = 200$. The numerical solutions corresponding to three values of N_s are plotted in Fig. 12. The pressure signals exhibit a significant phase error only for $N_s = 20$.

5.2. Test 2

A radial compact dipole is described as a small disk with a pressure jump uniformly distributed on its surface. One and three disks at a constant angle from each other are considered, rotating around a vertical axis at the frequency f_1 . The system translates at the velocity v_y , whereas the observer is fixed.

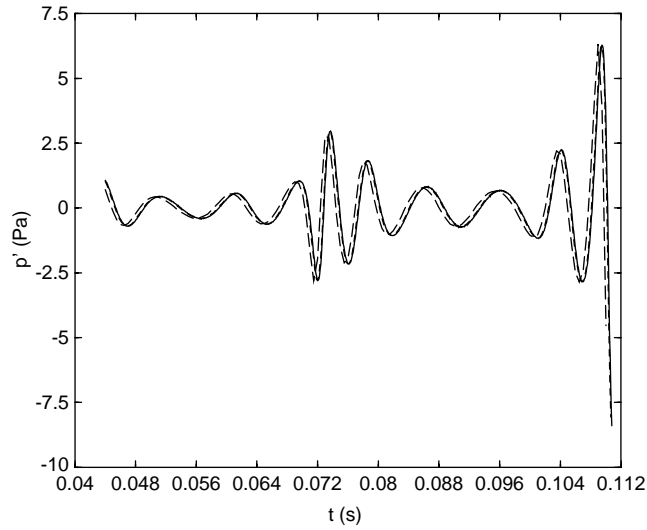


Fig. 12. Test 1, Case I. Numerical solutions for three values of the number of samples N_s per acoustic period: —, $N_s = 200, Err_{L2} = 8.24 \times 10^{-2}$; ----, $N_s = 75, Err_{L2} = 1.68 \times 10^{-1}$; - · -, $N_s = 20, Err_{L2} = 6.05 \times 10^{-1}$.

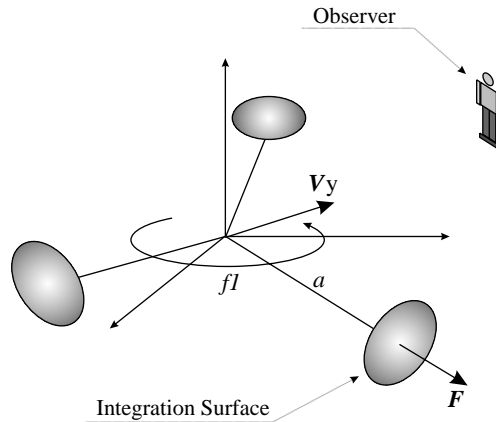


Fig. 13. Scheme of Test 2. A radial compact dipole is described as a small disk with a pressure jump uniformly distributed on its surface. One and three disks at a constant angle from each other are considered, rotating around a vertical axis at the frequency f_1 . The system translates at the velocity v_y , whereas the observer is fixed.

The sound radiated by a moving dipole is used as acoustic analytical solution (see Ref. [9, pp. 269–275]), namely

$$p'(\mathbf{x}, t) = \left[\frac{\mathbf{r} \cdot \dot{\mathbf{F}} - c\mathbf{M} \cdot \mathbf{F}}{4\pi cr^2(1 - M_r)^2} + (\mathbf{r} \cdot \mathbf{F}) \frac{\mathbf{r} \cdot \dot{\mathbf{M}} + c(1 - M^2)}{4\pi cr^3(1 - M_r)^3} \right]_{ret}, \tag{47}$$

where \mathbf{M} denotes the dipole Mach vector number and \mathbf{F} is the unsteady force exerted on the fluid. Dots on quantities denote time derivatives.

Several cases are considered in order to check the feasibility of an advanced time prediction of the noise from a subsonic high-speed rotor. The rotation frequency is kept constant at the value $f_1 = 10$ Hz, as well as the observer position $\mathbf{x} = (5, 4, 3)$ m. Different Mach numbers are obtained by varying both the radius a and the forward velocity \mathbf{v}_y . A point force of modulus $F = 1000$ N is introduced in the field through a pressure jump uniformly distributed on the surface of a small disk. This is obtained by flattening a sphere with a polar discretization of 5×5 elements³. One or three disks at a constant angle from each other are considered. The parameters for the different configurations are listed in Table 2.

Concerning the time discretization, 1000 time steps per rotation period are initially used for different configurations. Later on, computations are performed for one configuration down to 100 time steps per rotation period.

In Figs. 14–17, numerical results obtained with 1000 time steps per rotation period are checked against analytical solutions. The plots show that, as in Test 1, the agreement between the numerical and the analytical solutions is good for all the investigated configurations. The relative L-errors, as defined in Eq. (45), for the different configurations are listed in Table 2.

In Fig. 18, the relative L₂-error for Case H is plotted against the number of samples N_s per rotation period, from $N_s = 100$ up to 1000. The numerical solutions corresponding to three values of N_s are plotted in Fig. 19. The acoustic signatures show a significant phase error only for $N_s = 100$.

5.3. Test 3

An axial compact dipole is described as a small disk with a pressure jump uniformly distributed on its surface. Three and four disks at a constant angle from each other are considered, rotating around a vertical axis at the frequency f_1 . The system translates at the velocity \mathbf{v}_y , whereas the observer is fixed. Eq. (47) provides the acoustic analytical solution. In the present case, the force has a constant direction, providing $\dot{\mathbf{F}} = 0$.

As in Test 2, several cases are considered in order to check the feasibility of an advanced time rotor-noise prediction. The rotation frequency is kept constant at the value $f_1 = 10$ Hz, as well as the observer position $\mathbf{x} = (5, 4, 3)$ m. Different Mach numbers are obtained by varying both the radius a and the forward velocity \mathbf{v}_y . A point force of modulus $F = 1000$ N is introduced in the field through a pressure jump uniformly distributed on the surface of a small disk. This is obtained by flattening a sphere composed of 5×6 elements. Three or four disks at a constant angle from each other are considered. The parameters for the different configurations are listed in Table 3.

Concerning the time discretization, 1600 time steps per rotation period are initially used for different configurations. Later on, computations are performed for one configuration down to 160 time steps per rotation period.

In Figs. 21 and 22 numerical results obtained with 1600 time steps per rotation period are checked against analytical solutions. The plots show that, as in Tests 1 and 2, the agreement

³In this case, the surface discretization has no influence on the accuracy of the solution. Simply, it provides a further check of the Gaussian integration procedure and other coded libraries.

Table 2
Test 2: geometrical and kinematic parameters

	N	a	\mathbf{v}_y	M_y	Err_L	Fig.
A	1	1	(0,0,0)	0.18	7.10E-5	14(a)
B	3	1	(0,0,0)	0.18	1.17E-4	14(b)
C	1	3	(50,50,50)	0.81	6.49E-5	15(a)
D	3	3	(50,50,50)	0.81	2.59E-5	15(b)
E	1	5.4	(0,0,0)	0.998	1.03E-4	16(a)
F	3	5.4	(0,0,0)	0.998	1.25E-5	16(b)
G	1	2	(100,100,100)	0.88	7.35E-5	17(a)
H	3	2	(100,100,100)	0.88	1.24E-4	17(b)

N is the number of acoustic dipoles; a is the distance from the axis of rotation; \mathbf{v}_y is the translation velocity of the sources; M_y is the maximum Mach number of the integration surface; Err_L denotes the relative L-error; Fig. indicates the label of the corresponding figure. All the quantities are expressed in SI units. Computations are performed with a time discretization of 1000 time steps per rotation period.

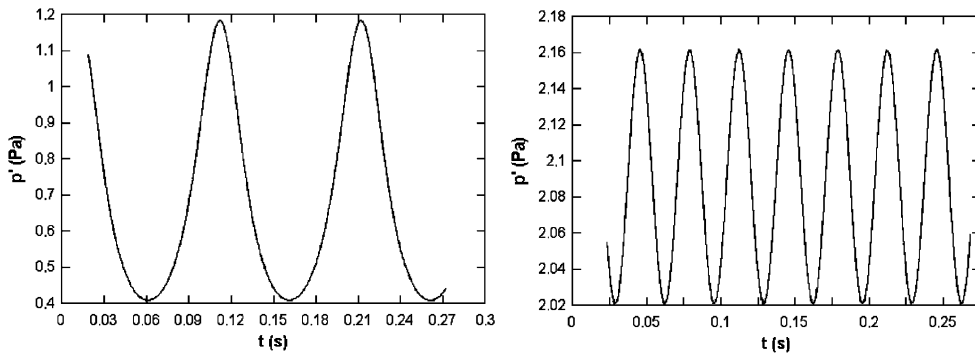


Fig. 14. Test 2. Case A (left) and Case B (right): —, analytical solution; ----, numerical solution.

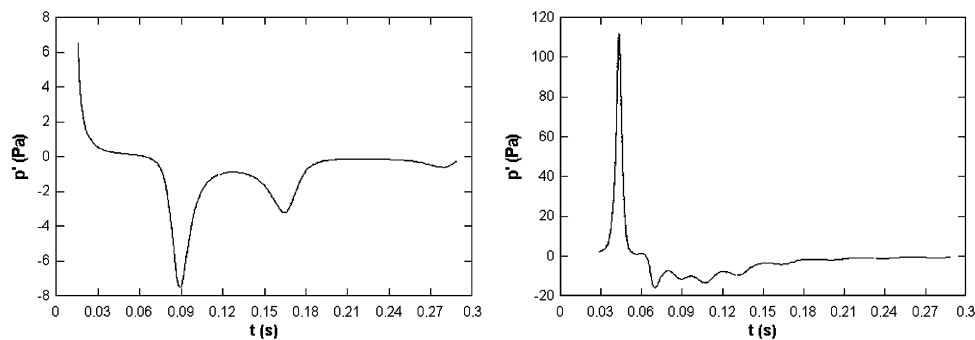


Fig. 15. Test 2. Case C (left) and Case D (right): —, Analytical solution; ----, numerical solution.

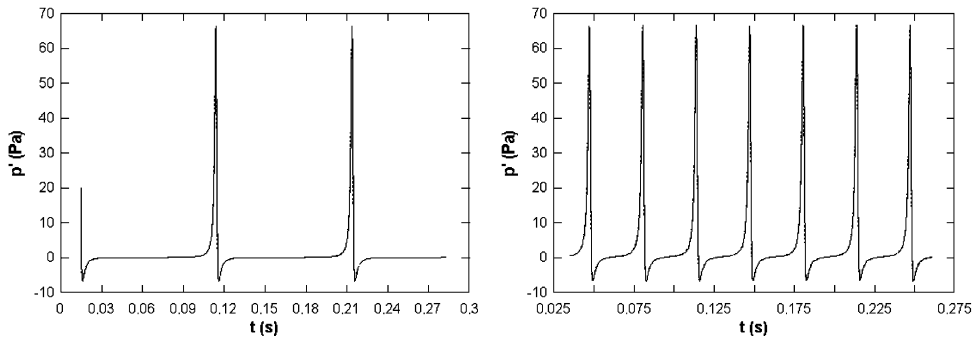


Fig. 16. Test 2. Case E (left) and Case F (right): —, Analytical solution; ----, numerical solution.

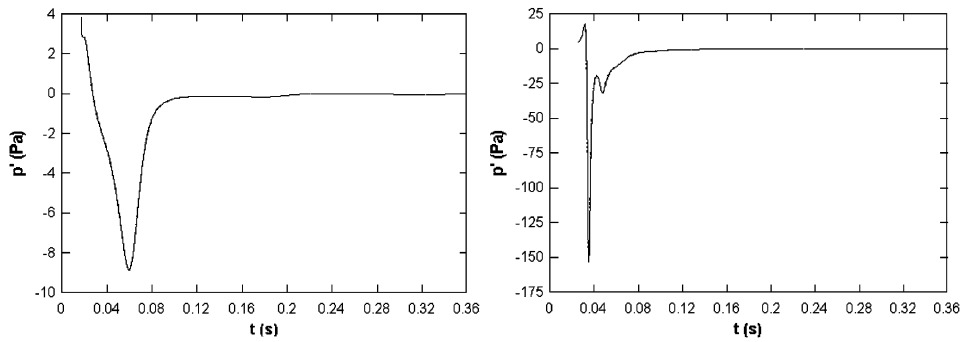


Fig. 17. Test 2. Case G (left) and Case H (right): —, Analytical solution; ----, numerical solution.

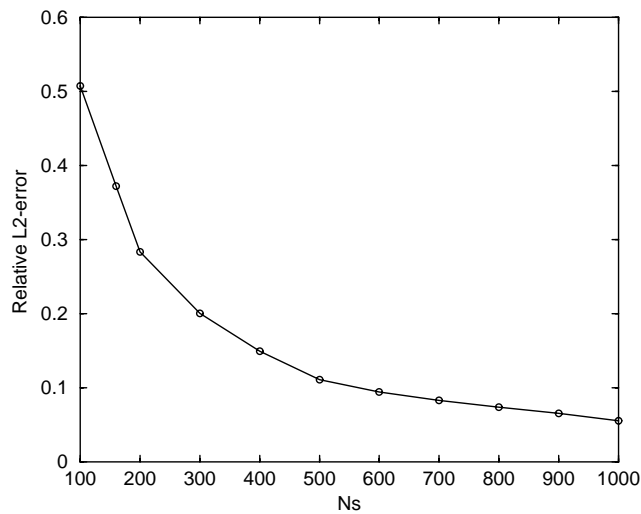


Fig. 18. Test 2, Case H. Relative L_2 -error versus the number of time steps per acoustic period.

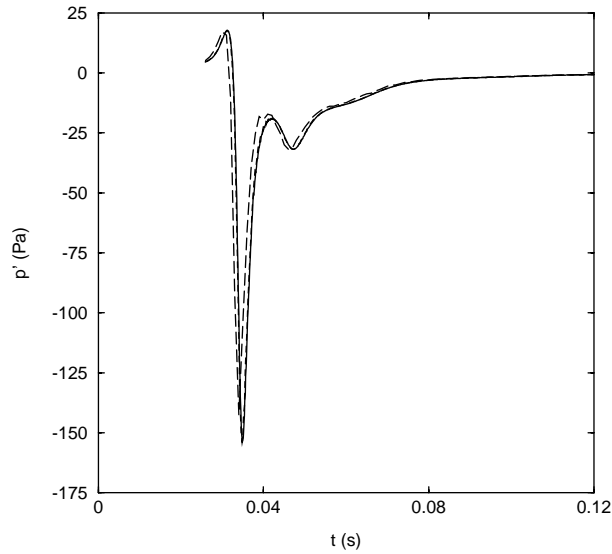


Fig. 19. Test 2, Case H. Numerical solutions for three values of the number of samples N_s per rotation period: —, $N_s = 1000, Err_{L2} = 5.56 \times 10^{-2}$; ---- $N_s = 500, Err_{L2} = 1.11 \times 10^{-1}$; -.- $N_s = 100, Err_{L2} = 5.07 \times 10^{-1}$.

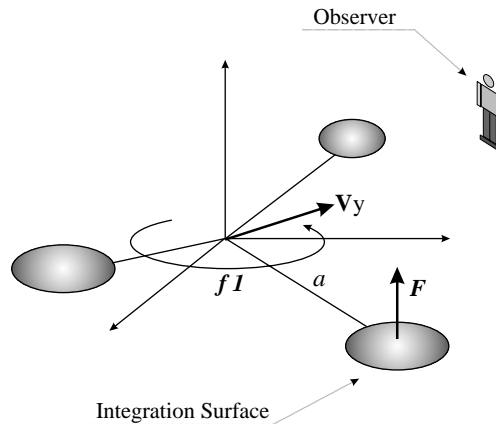


Fig. 20. Scheme of Test 3. An axial compact dipole is described as a small disk with a pressure jump uniformly distributed on its surface. Three and four disks at a constant angle from each other are considered, rotating around a vertical axis at the frequency f_1 . The system translates at the velocity v_y , whereas the observer is fixed.

between the numerical and the analytical solutions is good for all the investigated configurations. The relative L-errors, as defined in Eq. (45), for the different configurations are listed in Table 3.

In Fig. 23 the relative L_2 -error for Case D is plotted against the number of samples N_s per rotation period, from $N_s = 160$ up to 1600. The numerical solutions corresponding to three

Table 3
Test 3: geometrical and kinematic parameters

	N	a	\mathbf{v}_y	M_y	Err_L	Fig.
A	3	1	(0,0,0)	0.18	3.00E-3	21(a)
B	3	3	(0,0,0)	0.55	1.89E-5	21(b)
C	3	3	(100,100,0)	0.97	1.03E-3	22(a)
D	4	3	(100,100,0)	0.97	3.53E-4	22(b)

N is the number of acoustic dipoles; a is the distance from the axis of rotation; \mathbf{v}_y is the translation velocity of the sources; M_y is the maximum Mach number of the integration surface; Err_L denotes the relative L-error; Fig. indicates the label of the corresponding figure. All the quantities are expressed in SI units. Computations are performed with a time discretization of 1600 time steps per rotation period.

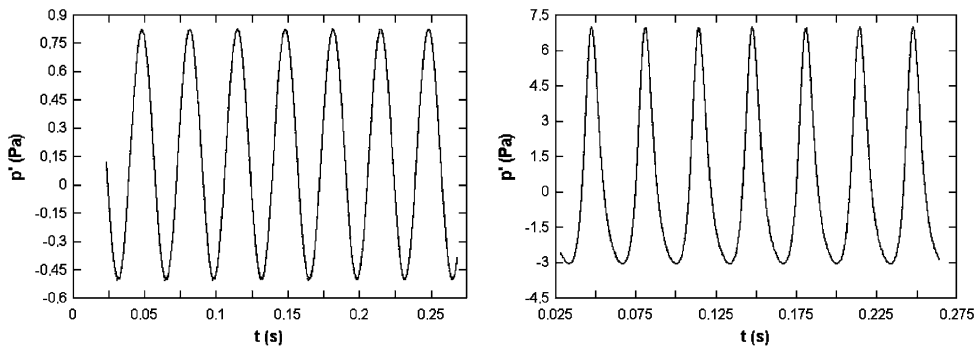


Fig. 21. Test 3. Case A (left) and Case B (right): —, analytical solution; ----, numerical solution.

values of N_s are plotted in Fig. 24. The pressure signals exhibit a small phase error only for $N_s = 160$.

6. Discussion

The feasibility of an advanced time aeroacoustic prediction has been proven through several test cases. The relative L-errors in Tables 1–3 show that a high level of accuracy has been obtained even in the case of surfaces moving at high Mach numbers, provided that a sufficient number of samples per period is used. Consistently, an increasing phase error appears as the time step is increased. This effect has been emphasized by evaluating the L_2 -error. Therefore, it has been shown that:

- The advanced time approach can be successfully applied to hybrid CFD/FW–H aeroacoustic predictions.
- The accuracy of the numerical prediction is not significantly affected by the kinematics of the problem, even at very high-source Mach numbers.

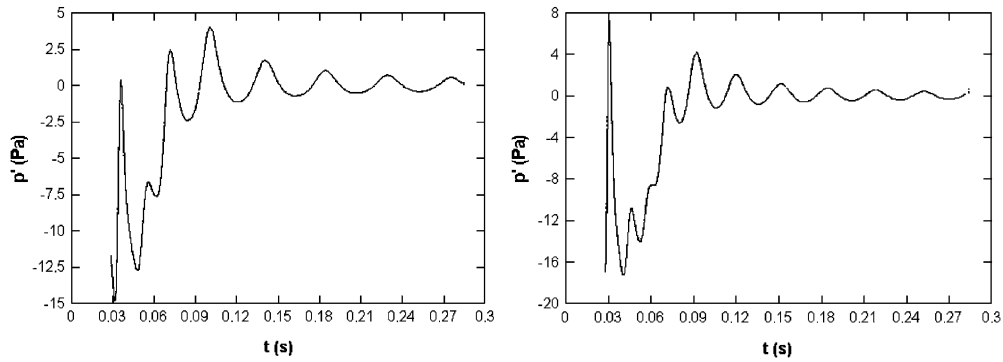


Fig. 22. Test 3. Case C (left) and Case D (right): —, analytical solution; ----, numerical solution.

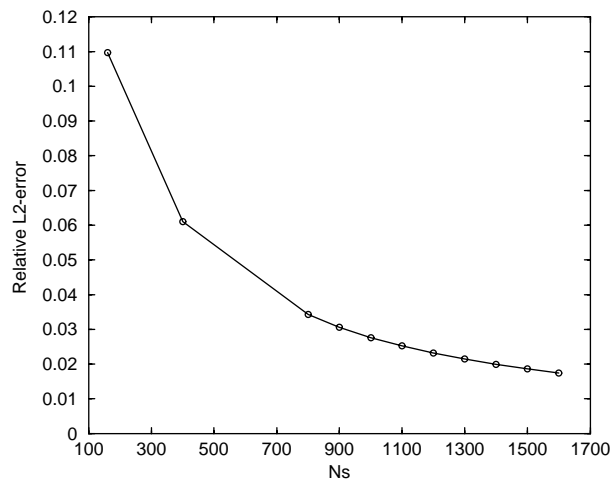


Fig. 23. Test 2, Case H. Relative L_2 -error versus the number of time-steps per acoustic period.

- The FW–H integral formulation based on a penetrable control surface provides consistent results even when the integration surface rotates and translates at high velocities. The definition of the aerodynamic quantities and their time derivatives on a rotating penetrable surface is a complicated matter. Therefore the test cases herein discussed constitute an original aspect of the present work.
- The thickness noise extension to a moving observer is consistent with an advanced time approach.

The *acoustic* assessment of *Advantia* can be successfully concluded with the awareness that: the thickness and the loading noise contributions from a high-speed (subsonic) surface can be accurately predicted through an advanced time formulation, which is more effective and simple than a classic retarded time formulation.

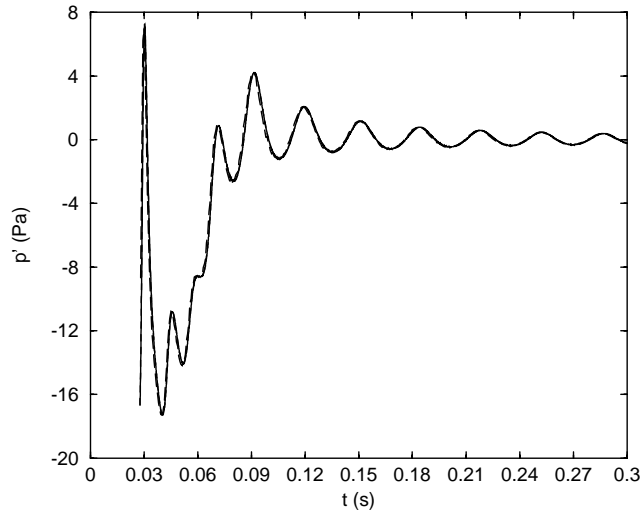


Fig. 24. Test 3, Case D. Numerical solutions for three values of the number of samples N_s per rotation period: —, $N_s = 1600$, $Err_{L2} = 1.74 \times 10^{-2}$; ----, $N_s = 1100$, $Err_{L2} = 2.52 \times 10^{-2}$; - · -, $N_s = 160$, $Err_{L2} = 1.10 \times 10^{-1}$.

7. Conclusions

In this paper it has been shown that a retarded time solution of a generic wave equation can be computed through an advanced time approach.

When applied to the aerodynamic noise prediction, the advanced time formulation allows one to build progressively the time trace of the radiated acoustic pressure by using aerodynamic data as early as these are computed by an aerodynamic solver. Hence, the traditional concept of a post-process acoustic prediction is partially bypassed. The practical advantages offered by this methodology are:

- the feasibility of an aeroacoustic prediction running parallelly to an aerodynamic prediction;
- no disk recordings of the aerodynamic data are necessary for the sake of an aeroacoustic prediction;
- the advanced time is an algebraic function of the observer and point source location at the emission time. Therefore, no iterative solutions of the retarded time equation must be performed, resulting in an increased efficiency of the numerical algorithms.

Minor results of the present study are:

- the thickness noise extension to a moving observer with time derivatives taken inside the integrals;
- a formulation of the integral FW–H equation in terms of dimensionless quantities, with velocities defined in the body reference frame.

Non-trivial test cases were performed in order to assess the consistency of the advanced time formulation. These were chosen in order to test all the numerical procedures involved in a rotor noise prediction.

No attempt was made in the present work to exploit the advanced time approach in the transonic regime. Nevertheless, we believe that an examination of the transonic singularity in the spirit of an advanced time prediction could suggest the way of an ad hoc treatment of this regime.

As a final remark, the feasibility of an acoustic prediction running parallelly to an aerodynamic prediction could be of primary importance in the evaluation of volume contributions.

Appendix A. Interpolation scheme in the advanced time domain

In this appendix, the procedure used in the present study to build on the acoustic signal in the advanced time domain is described.

At each source time step j and for each source element i , the advanced time t_{adv}^j and the corresponding elementary sound contribution p' are computed. Then, the quantities

$$j_{adv} = \text{int} \left(\frac{t_{adv}^j}{\Delta t} \right), \quad (\text{A.1})$$

$$w = \frac{t_{adv}^j}{\Delta t} - j_{adv}, \quad (\text{A.2})$$

are computed, j_{adv} denoting the advanced time step and w the normalized difference between t_{adv}^j and the discrete advanced time $j_{adv}\Delta t$.

Later on, the elementary sound contribution p_i^j is computed by means of a case procedure which depends on whether a contribution p_i^j has been already computed or not, that is

(1) if $p_i^j = 0$ (not computed), then

$$p_i^j = p', \quad (\text{A.3})$$

$$w_i^j = w, \quad (\text{A.4})$$

(2) if $p_i^j \neq 0$ (already computed), then

$$p_w = \frac{p_i^j - p'}{w_i^j - w}, \quad (\text{A.5})$$

$$p_i^j = p' - p_w w, \quad (\text{A.6})$$

$$w_i^j = 0. \quad (\text{A.7})$$

Both the values of p_i^j and w_i^j are stored. It is straightforward to verify that, once $w_i^j = 0$ has been set by a first execution of block (2), successive executions do not affect the value of p_i^j .

Finally, a summation over all the source elements, say $p^j = \sum_i p_i^j$, provides the pressure value at the advanced time-step j_{adv} .

Appendix B. Symbols used in the FW–H formulation

The aerodynamic field is introduced in Eqs. (27)–(29) in terms of conservative variables, namely, the flow density ρ , the linear momentum $\rho\tilde{u}_i$, \tilde{u}_i being the relative velocity of the flow with respect to the integration surface $f = 0$, the specific total internal energy ρE and the specific turbulent kinetic energy ρK . A description of all the involved quantities is reported below:

$$\begin{aligned}
 p_d &= \frac{1}{2}\rho_0 U_{ref}^2, & \theta &= tU_{ref}/l_{ref}, & M_{ref} &= U_{ref}/c, & V_i &= v_i/U_{ref}, & V_n &= V_i\hat{n}_i, \\
 \mathbf{X} &= \mathbf{x}/l_{ref}, & \mathbf{Y} &= \mathbf{y}/l_{ref}, & \hat{r}_i &= \frac{X_i - Y_i}{|\mathbf{X} - \mathbf{Y}|}, & R &= |\mathbf{X} - \mathbf{Y}|, \\
 M_i &= v_i/c, & M_r &= M_i\hat{r}_i, & \dot{M}_r &= \dot{M}_i\hat{r}_i, & \ddot{M}_r &= \ddot{M}_i\hat{r}_i, & M_{or} &= M_{oi}\hat{r}_i, \\
 \tilde{u}_i &= u_i - v_i, & \sigma &= \frac{\rho}{\rho_0}, & q_i &= \frac{(\rho\tilde{u}_i)}{(\rho_0 U_{ref})}, & e &= \frac{(\rho E)}{(\rho_0 U_{ref}^2)}, & k &= \frac{(\rho K)}{(\rho_0 U_{ref}^2)}, \\
 C_p &= 2\left\{(\gamma - 1)\left[e - \frac{q_i q_i}{2\sigma} - k\right] - \frac{p_0}{2p_d}\right\} \\
 \dot{C}_p &= 2(\gamma - 1)\left[\dot{e} - \frac{q_i \dot{q}_i}{\sigma} + \dot{\sigma} \frac{q_i q_i}{2\sigma^2} - \dot{k}\right], \\
 \lambda_i &= \frac{C_p}{2}\hat{n}_i + V_i q_n + \frac{q_i q_n}{\sigma}, \\
 \chi_i &= \frac{\dot{C}_p}{2}\hat{n}_i + \frac{C_p}{2}\dot{\hat{n}}_i + \dot{V}_i q_n + V_i(\dot{q}_i \hat{n}_i) + V_i(q_i \dot{\hat{n}}_i) \\
 &\quad + \frac{\dot{q}_i q_n}{\sigma} + \frac{q_i(\dot{q}_i \hat{n}_i)}{\sigma} + \frac{q_i(q_i \dot{\hat{n}}_i)}{\sigma} - \frac{q_i q_n \dot{\sigma}}{\sigma^2}, \\
 \Psi_{ij} &= \frac{q_i q_j}{\sigma} + \sigma V_i V_j + q_i V_j + q_j V_i + \left(\frac{C_p}{2} - \frac{\sigma - 1}{M_{ref}^2}\right)\delta_{ij}, \\
 q_n &= q_i \hat{n}_i, & \lambda_M &= \lambda_i M_i, & \lambda_r &= \lambda_i \hat{r}_i, & \lambda_r &= \chi_i \hat{r}_i, \\
 \Psi_{MM} &= \Psi_{ij} M_i M_j, & \Psi_{Mr} &= \Psi_{ij} M_i \hat{r}_j, & \Psi_{\dot{M}r} &= \Psi_{ij} \dot{M}_i \hat{r}_j, & \Psi_{rr} &= \Psi_{ij} \hat{r}_i \hat{r}_j, \\
 \dot{\Psi}_{Mr} &= \dot{\Psi}_{ij} M_i \hat{r}_j, & \dot{\Psi}_{rr} &= \dot{\Psi}_{ij} \hat{r}_i \hat{r}_j, & \ddot{\Psi}_{rr} &= \ddot{\Psi}_{ij} \hat{r}_i \hat{r}_j.
 \end{aligned}$$

In these expressions, p_0 and ρ_0 are the quiescent fluid pressure and density, respectively, M_o denotes the observer Mach number, \hat{n}_i is the unit vector pointing out of the integration surface and upper dots denote derivatives with respect to the dimensionless time θ . The loading-noise term χ_i is the dimensionless time derivative of λ_i . In a similar way, both $\dot{\Psi}_{ij}$ and $\ddot{\Psi}_{ij}$ can be obtained from the quadrupole noise term Ψ_{ij} .

Appendix C. Nomenclature

c	sound speed in quiescent medium
C_p	pressure coefficient
$H(), \delta()$	Heaviside and Dirac functions

K	turbulent kinetic energy
l_{ref}	reference length
E	total internal energy
M_i	Mach number of the surface $f = 0$
M_{ref}, U_{ref}	reference Mach number and reference velocity
M_{oi}	observer Mach number vector
M_{or}	observer Mach number vector in the radiation direction
\hat{n}_i	unit outward normal vector to the integration surface
p_0	pressure in quiescent medium
p', ρ'	pressure and density disturbances
p_d	reference dynamic pressure
R	dimensionless distance between observation and source points
\hat{r}_i	radial unit vector
t, θ	time and dimensionless time
T_{ij}	Lighthill's stress tensor
u_i	flow velocity
\tilde{u}_i	flow velocity relative to the integration surface
v_i, V_i	velocity and dimensionless velocity of the surface $f = 0$
\mathbf{x}, \mathbf{X}	observer position and dimensionless observer position
\mathbf{y}, \mathbf{Y}	source position and dimensionless source position
δ_{ij}	Kronecker delta
γ	specific heat ratio
λ_i, χ_i	loading noise source terms
$\rho, \rho u_i, \rho E, \rho K$	aerodynamic conservative quantities
ρ_0	flow density in quiescent medium
ρ	flow density
σ, q_i, e, k	dimensionless aerodynamic conservative quantities
τ_{ij}	viscous stress tensor
Ψ_{ij}	quadrupole noise source terms
\square^2	wave operator

Superscripts

\cdot time derivative

Subscripts

n projection in the normal direction
 r projection in the radiation direction

Abbreviations

BEM Boundary Element Method
 CAA Computational AeroAcoustics
 CFD Computational Fluid Dynamics
 FW-H Ffowcs-Williams and Hawkings
 RANS Reynolds-Averaged Navier Stokes

References

- [1] M.J. Lighthill, On sound generated aerodynamically: 1. general theory, *Proceeding of The Royal Society A* 211 (1952) 564–578.
- [2] J.E. Ffowcs Williams, D.L. Hawkings, Sound generated by turbulence and surfaces in arbitrary motion, *Philosophical Transactions of the Royal Society A* 264 (1969) 321–342.
- [3] P. di Francescantonio, A new boundary integral formulation for the prediction of sound radiation, *Journal of Sound and Vibration* 202 (4) (1997) 491–509.
- [4] K.S. Brentner, F. Farassat, Analytical comparison of the acoustic analogy and Kirchhoff formulation for moving surfaces, *American Institute of Aeronautics and Astronautics Journal* 36 (8) (1998) 1379–1386.
- [5] F. Farassat, G.P. Succi, The prediction of helicopter discrete frequency noise, *Vertica* 7 (4) (1983) 309–320.
- [6] K.S. Brentner, An efficient and robust method for predicting helicopter high-speed impulsive noise, *Journal of Sound and Vibration* 203 (1) (1997) 87–100.
- [7] F. Farassat, Theory of noise generation from moving bodies with an application to helicopter rotors, NASA Technical Report R-451, 1975.
- [8] H. Ardavan, The breakdown of the linearized theory and the role of quadrupole sources in transonic rotor acoustics, *Journal of Fluid Mechanics* 226 (1991) 591–624.
- [9] S.W. Rienstra, A. Hirschberg, An introduction to acoustics, Extended and revised edition of Report IWDE92-06, Technische Universiteit Eindhoven, 2001.